Stable parity-time-symmetric nonlinear modes and excitations in a derivative nonlinear Schrödinger equation

Yong Chen and Zhenya Yan*

Key Laboratory of Mathematics Mechanization, Institute of Systems Science, AMSS, Chinese Academy of Sciences, Beijing 100190, China and University of Chinese Academy of Sciences, Beijing 100049, China

(Received 21 May 2016; revised manuscript received 16 July 2016; published 13 January 2017)

The effect of derivative nonlinearity and parity-time-symmetric ($\mathcal{PT}$-symmetric) potentials on the wave propagation dynamics is explored in the derivative nonlinear Schrödinger equation, where the physically interesting Scarf-II and harmonic-Hermite-Gaussian potentials are chosen. We study numerically the regions of unbroken and broken linear $\mathcal{PT}$-symmetric phases and find some stable bright solitons of this model in a wide range of potential parameters even though the corresponding linear $\mathcal{PT}$-symmetric phases are broken. The semielastic interactions between particular bright solitons and exotic incident waves are illustrated such that we find that particular nonlinear modes almost keep their shapes after interactions even if the exotic incident waves have evidently been changed. Moreover, we exert the adiabatic switching on $\mathcal{PT}$-symmetric potential parameters such that a stable nonlinear mode with the unbroken linear $\mathcal{PT}$-symmetric phase can be excited to another stable nonlinear mode belonging to the broken linear $\mathcal{PT}$-symmetric phase.

DOI: 10.1103/PhysRevE.95.012205

I. INTRODUCTION

The famous derivative nonlinear Schrödinger (DNLS) equation possesses the following normalized form [1]

$$i\psi_t + \psi_{xx} + ig(|\psi|^2\psi)_x = 0, \quad g > 0, \tag{1}$$

where the subscripts denote the partial derivatives with respect to the variables, g represents the relative magnitude (the space-reflection transformation $x \to -x$ can make $g < 0$) of the derivative nonlinearity term, which is also called the nonlinear dispersion term [1]. In fact, Eq. (1) has a close relation with the modified nonlinear Schrödinger (MNLS) equation [2,3]

$$iq_\xi + \alpha q_{\tau\tau} + \lambda|q|^2 q + i\gamma(|q|^2 q)_\tau = 0, \tag{2}$$

where α denotes the group velocity dispersion coefficient, the Kerr nonlinear coefficient λ and derivative nonlinear coefficient γ both depend on nonlinear refractive index n_2. Equation (2) can be transformed into Eq. (1) by using the similarity (or gauge) transformation [4]

$$q(\tau,\xi) = \psi(x,t)e^{i(kx+k^2t)}$$

with $x = \frac{\gamma}{\alpha g}\tau - \frac{2\lambda}{g}\xi$, $t = \frac{\gamma^2}{\alpha g^2}\xi$, and $k = \frac{\alpha g\lambda}{\gamma^2}$.

Equation (1) [or the similarity Eq. (2)] can be used to describe many nonlinear wave phenomena in some physical applications such as the propagations of small-amplitude nonlinear Alfvén waves in a low-β plasma [5], large-amplitude magnetohydrodynamic waves propagating in an arbitrary direction with respect to the magnetic field in a high-β plasma [6], the filamentation of lower-hybrid waves [7], and the subpicosecond or femtosecond pulses in single-mode optical fiber [2,3]. Equation (1) can be solved using the inverse scattering method [8]. Moreover, some modified models [e.g., Eq. (2)] had been studied in detail such as the Chen-Li-Liu equation [9] and the modified NLS equation [4,9–11]. Particularly, the localized solutions and dynamics in the Raman-extended DNLS equation were also studied analytically and numerically [12,13].

The NLS equation describing light propagation in optics [14] with real external potentials and/or gain-and-loss distributions has been investigated [15–31] since the refractive index of the optical waveguide can be complex [32,33]. It is surprising to find that if the complex refractive index satisfies the property of the parity-time ($\mathcal{PT}$) symmetry [34]: $\mathcal{P}: x \to -x; \mathcal{T}: i \to -i$, that is, if the real and imaginary parts of the refractive index are the even and odd functions of spatial position, respectively, then the propagation constant of the light can still be in all-real spectrum range, hence admitting stationary beam transmission [35–38]. Moreover, the complex $\mathcal{PT}$-symmetric potentials can also support continuous families of stable solitons [20–31] even if the solitons appear in the range of the broken linear $\mathcal{PT}$-symmetric phases (see, e.g., Ref. [21]). More recently, the stable nonlinear modes were found in the third-order NLS equation with $\mathcal{PT}$-symmetric potentials [39]. Other interesting $\mathcal{PT}$-symmetric phenomena or properties can be found in the relevant theoretical and experimental studies [36,37,40–42].

It is still a significant subject to explore whether stable nonlinear modes exist in other nonlinear physical models with $\mathcal{PT}$-symmetric potentials. To the best of our knowledge, soliton dynamics of the DNLS equation (1) in the $\mathcal{PT}$-symmetric potentials was not studied before, which can be regarded as an extension of the NLS equation with $\mathcal{PT}$-symmetric potentials (see, e.g., Refs. [20–22]). Our main goal in this paper is to find stable solitons and study their exciting behaviors of the DNLS equation (1) in two kinds of physically interesting $\mathcal{PT}$-symmetric potentials (i.e., $\mathcal{PT}$-symmetric Scarf-II and harmonic-Hermite-Gaussian potentials).

The rest of this paper is arranged as follows. We first present the broken and unbroken regions of the linear spectral problem with some physically interesting $\mathcal{PT}$-symmetric potentials. Then we analyze the effect of the $\mathcal{PT}$-symmetric potentials and derivative nonlinearity on the stability, wave propagations, interactions, transverse power-flow density of solitons in

*Corresponding author: zyyan@mmrc.iss.ac.cn

detail. Finally, based on the adiabatic change technique we also perform some types of stable excitations belonging to the broken linear $\mathcal{PT}$-symmetric phases from nonlinear modes.

II. NONLINEAR PHYSICAL MODEL WITH $\mathcal{PT}$-SYMMETRIC POTENTIALS

A. Nonlinear wave equation

We begin our investigation by considering the propagation of optical waves in the derivative nonlinearity and $\mathcal{PT}$-symmetric potential. The light evolution can be modeled by the following normalized derivative nonlinear Schrödinger-like equation with $\mathcal{PT}$-symmetric potential

$$i\psi_t + \psi_{xx} - [V(x) + iW(x)]\psi + ig(|\psi|^2\psi)_x = 0, \quad (3)$$

where $\psi = \psi(x,t)$ is a complex wave function of x,t, which is proportional to the electric field envelope, t denotes the scaled propagation time or distance, x represents the normalized transverse coordinate, and g is a positive nonlinear coefficient (without loss of generality we can choose $g = 1$). The $\mathcal{PT}$-symmetric potential $V(x) + iW(x)$ requires that its real and imaginary components satisfy $V(-x) = V(x)$ and $W(-x) = -W(x)$ describing the real-valued external potential and gain-and-loss distribution, respectively. Similar to the NLS equation with $\mathcal{PT}$-symmetric potentials [20], the $\mathcal{PT}$-symmetric potential in Eq. (3) can be achieved by a judicious inclusion of gain or loss regions in guided wave geometries [44,45]. Recently, the effect of the shock-induced $\mathcal{PT}$-symmetric potentials was studied by considering the coupled derivative NLS equations [42], which are relevant to Eq. (3). When we make the transformation $t \to z$ (propagation distance) and $x \to t$ (propagation time), Eq. (3) may be used to describe the evolution of pulses inside a single-mode fiber [1,43].

It is easy to show that Eq. (3) is invariant under the $\mathcal{PT}$-symmetric transformation if the complex potential $[V(x) + iW(x)]$ is $\mathcal{PT}$ symmetric, where $\mathcal{P}$ and $\mathcal{T}$ operators are defined by $\mathcal{P}: x \to -x; \mathcal{T}: i \to -i, t \to -t$. Equation (3) can be rewritten as the form $\psi_t = -\frac{\partial}{\partial x}\frac{\delta \mathcal{H}}{\delta \psi^*}$ with the Hamiltonian $\mathcal{H} = \int_{-\infty}^{+\infty}\{-i\psi^*\psi_x + \psi^*\int_0^x [iV(x) - W(x)]\psi dx + \frac{g}{2}|\psi|^4\}dx$, where the asterisk stands for the complex conjugate. The power and quasipower [20] of Eq. (3) are given by $P(t) = \int_{-\infty}^{+\infty}|\psi(x,t)|^2 dx$ and $Q(t) = \int_{-\infty}^{+\infty}\psi(x,t)\psi^*(-x,t)dx$, respectively. One can immediately obtain that $P_t = 2\int_{-\infty}^{+\infty} W(x)|\psi(x,t)|^2 dx$ and $Q_t = -\int_{-\infty}^{+\infty} g\psi(x,t)\psi^*(-x,t)\{(|\psi(x,t)|^2)_x - [|\psi(-x,t)|^2]_x + \psi^*(x,t)\psi_x(x,t) - \psi(-x,t)\psi_x^*(-x,t)\}dx$.

B. General theory

The stationary solutions of Eq. (3) are considered in the form $\psi(x,t) = \phi(x)e^{i\mu t}$, where μ is the real propagation constant and the nonlinear localized eigenmode [$\lim_{|x|\to\infty}\phi(x) = 0$] satisfies

$$\frac{d^2\phi}{dx^2} - [V(x) + iW(x)]\phi + ig\frac{d(|\phi|^2\phi)}{dx} = \mu\phi. \quad (4)$$

For Eq. (4) with some functions $V(x)$ and $W(x)$, there exist two cases for the study of solutions of Eq. (4):

(i) if $\phi(x)$ is a real-valued function, then we have the general solution of Eq. (4)

$$\phi^2(x) = \frac{2}{3g}\partial_x^{-1}W(x), \quad (5)$$

with the condition linking the potential and gain-and-loss distribution being

$$W^2(x) - 2W_x(x)\partial_x^{-1}W(x) + 4[V(x)+\mu]\left[\partial_x^{-1}W(x)\right]^2 = 0, \quad (6)$$

where $\partial_x^{-1}W(x) = \int_0^x W(s)ds$.

(ii) if the function $\phi(x)$ is complex in the form

$$\phi(x) = \rho(x)\exp\left[i\int_0^x v(s)ds\right], \quad (7)$$

where $\rho(x)$ is the real amplitude, and the real function $v(x)$ is the hydrodynamic velocity [46], then we substitute Eq. (7) into Eq. (4) and separate the real and imaginary parts to yield the relations linking the hydrodynamic velocity

$$v(x) = \rho^{-2}(x)\int_0^x W(s)\rho^2(s)ds - \frac{3g}{4}\rho^2(x), \quad (8)$$

and the amplitude satisfying the second-order ordinary differential equation with varying coefficients

$$\frac{d^2\rho(x)}{dx^2} = [V(x) + v^2(x) + \mu]\rho(x) + gv(x)\rho^3(x). \quad (9)$$

To further study the linear stability of such nonlinear localized modes $\psi(x,t) = \phi(x)e^{i\mu t}$, we consider the perturbed solutions of Eq. (3) as follows:

$$\psi(x,t) = \{\phi(x) + \epsilon[F(x)e^{i\delta t} + G^*(x)e^{-i\delta^* t}]\}e^{i\mu t}, \quad (10)$$

where $\epsilon \ll 1, F(x)$ and $G(x)$ are the perturbation eigenfunctions of the linearized eigenvalue problem and δ measures the growth rate of the perturbation instability. Substituting Eq. (10) into Eq. (3) and linearizing with respect to ϵ, we obtain the following linear eigenvalue problem for the perturbation modes

$$\begin{pmatrix} \hat{L}_1 & \hat{L}_2 \\ -\hat{L}_2^* & -\hat{L}_1^* \end{pmatrix}\begin{pmatrix} F(x) \\ G(x) \end{pmatrix} = \delta\begin{pmatrix} F(x) \\ G(x) \end{pmatrix}, \quad (11)$$

where

$$\hat{L}_1 = \partial_x^2 + 2ig[|\phi|^2\partial_x + (|\phi|^2)_x] - [V(x) + iW(x)] - \mu,$$

and

$$\hat{L}_2 = ig[\phi^2\partial_x + (\phi^2)_x].$$

Obviously, the $\mathcal{PT}$-symmetric nonlinear modes are linearly stable if δ is purely real, otherwise they are linearly unstable.

In what follows we study Eqs. (3) and (4) analytically and numerically in detail for two distinct physically interesting $\mathcal{PT}$-symmetric potentials.

III. NONLINEAR MODES IN THE $\mathcal{PT}$-SYMMETRIC SCARF-II POTENTIAL

The first potential to consider is the celebrated $\mathcal{PT}$-symmetric Scarf-II potential [20,21,38]

$$V(x) = V_0\mathrm{sech}^2 x, \quad W(x) = W_0\mathrm{sech}x\tanh x, \quad (12)$$

where the real parameters $V_0 < 0$ and W_0 modulate the amplitudes of the reflectionless potential $V(x)$ and gain-and-loss distribution $W(x)$, respectively. For the case $W_0 > 0, W(x)$ represents the gain (loss) action in the domain of $x \geqslant 0$ ($x \leqslant 0$), respectively, whereas $W_0 < 0, W(x)$ represents the gain (loss) action in the domain of $x \leqslant 0$ ($x \geqslant 0$), respectively. Evidently, both $V(x)$ and $W(x)$ are bounded and vanish as $|x| \to \infty$. Moreover, the gain-and-loss distribution $W(x)$ always has a global balance in Eq. (3) since $\int_{-\infty}^{+\infty} W(x)dx = 0$.

A. Linear spectral problem

In the absence of the derivative nonlinearity ($g = 0$), Eq. (4) becomes the following linear eigenvalue problem with the $\mathcal{PT}$-symmetric Scarf-II potential (12)

$$L\Phi(x) = \lambda\Phi(x), \quad L = -\partial_x^2 + V(x) + iW(x), \tag{13}$$

with λ and $\Phi(x)$ being the eigenvalue and localized eigenfunction, respectively. By virtue of the spectral method, we numerically find its symmetry-breaking line in (V_0, W_0) space, which coincides well with the theoretical result that Eq. (13) with Eq. (12) enjoys entirely real spectra provided that $|W_0| \leqslant -V_0 + 1/4$ [38] [see Fig. 1(a)]. Therefore, for a fixed W_0 satisfying $|W_0| > 1/4$, there always exists a threshold of the potential amplitude V_0, beyond which a phase transition occurs and the corresponding spectra become complex in the meantime [see Figs. 1(b), 1(c)].

However, more interestingly, even though the phase transition occurs in the linear spectral problem [i.e., Eq. (13) has the complex spectra], nonlinear modes can still exist with entirely real eigenvalues, since the beam itself can have a strong influence on the amplitude of the potential through the derivative nonlinearity. Thus, for the same parameter W_0, the new effective potential with stronger derivative nonlinearity may alter the linear $\mathcal{PT}$-symmetric threshold with the result that nonlinear eigenmodes can be found with real eigenvalues. But the broken $\mathcal{PT}$ symmetry cannot be nonlinearly restored at the lower power levels subject to the weaker derivative nonlinearity. Thus, in what follows we turn to investigate nonlinear modes of Eq. (3) with $\mathcal{PT}$-symmetric Scarf-II potential (12) analytically and numerically.

B. Stability and dynamics of nonlinear modes

Without loss of generality, we consider $g = 1$ in Eq. (4). The particular (bright) soliton solutions (similarly hereafter) of Eq. (4) with the Scarff-II potential (12) can be found in the form

$$\phi(x) = \sqrt{\tfrac{2}{3}\phi_0 \,\mathrm{sech}x}\, \exp[i\varphi(x)], \tag{14}$$

where $\phi_0 = W_0 \pm \sqrt{4W_0^2 + 12V_0 + 9} > 0$ with $4W_0^2 + 12V_0 + 9 \geqslant 0$ [cf. Eq. (7); "+" denotes Scarf-II-Case-1 and "−" Scarf-II-Case-2, hereafter], the propagation constant is $\mu = 0.25$, and the nontrivial phase is

$$\varphi(x) = -\frac{(W_0 + \phi_0)}{2}\tan^{-1}(\sinh x).$$

It is easy to know that the above-mentioned condition, $\phi_0 = W_0 \pm \sqrt{4W_0^2 + 12V_0 + 9} > 0$ with $4W_0^2 + 12V_0 + 9 \geqslant 0$, yields the existence conditions for the bright solitons (14)

$$V_0 > -\tfrac{1}{4}\left(W_0^2 + 3\right) \quad \text{for} \quad W_0 < 0, \tag{15a}$$

or

$$V_0 > -\left(\frac{W_0^2}{3} + \frac{3}{4}\right) \quad \text{for} \quad W_0 > 0, \tag{15b}$$

for the Scarf-II-Case-1 and

$$-\left(\frac{W_0^2}{3} + \frac{3}{4}\right) \leqslant V_0 < -\frac{1}{4}\left(W_0^2 + 3\right) \quad \text{for} \quad W_0 > 0 \tag{16}$$

for the Scarf-II-Case-2. Apparently, the nonlinear localized modes (14) are also $\mathcal{PT}$ symmetric. It is easy to see that for the same $\mathcal{PT}$-symmetric potential, the solutions (14) of the DNLS equation and ones of NLS equation (see Refs. [20,21]) have the distinct properties.

It is easy to see from Fig. 1(a) that except for the only one tangent point $(V_0, W_0) = (-0.75, 0)$, the dashed parabola $V_0 = -(W_0^2/3 + 0.75)$ is completely contained in the solid parabola $V_0 = -0.25(W_0^2 + 3)$, which is tangent with the two linear $\mathcal{PT}$-symmetric breaking lines $\pm W_0 = 0.25 - V_0$ with two tangent points being $(V_0, W_0) = (-1.75, \pm 2)$. Thus, the existence region of bright solitons (14) for Scarf-II-Case-1

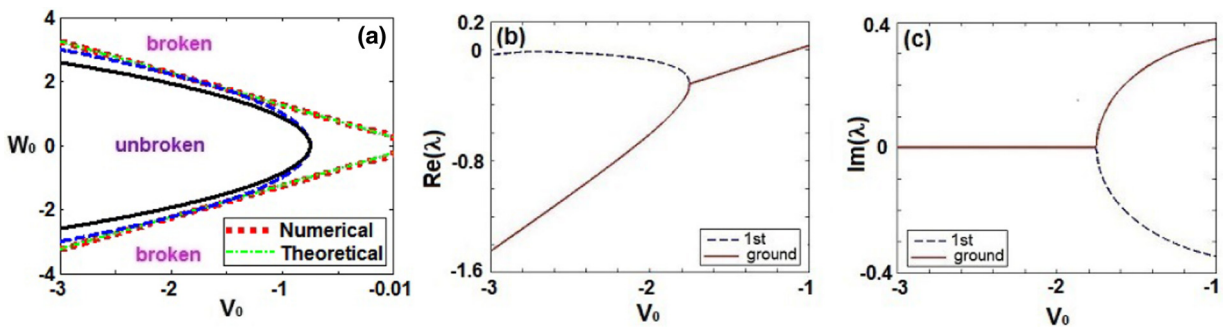

FIG. 1. (a) The unbroken (broken) $\mathcal{PT}$-symmetric phase is in the domain inside (outside) two phase breaking lines (the theoretically dash-dotted green and the numerically dotted red coincide by and large) for the linear operator L in Eq. (13) with $\mathcal{PT}$-symmetric Scarf-II potentials (12), where the dashed blue parabola is $W_0^2 + 4V_0 + 3 = 0$ (similarly hereinafter), whose tangent points with the two phase-breaking lines above are $(V_0, W_0) = (-1.75, \pm 2)$, and the solid parabola is $4W_0^2 + 12V_0 + 9 = 0$ (similarly hereinafter), which is tangent with the dashed parabola at $(V_0, W_0) = (-0.75, 0)$. (b) Real and (c) imaginary parts of the first two eigenvalues λ of the linear problem (13) with $\mathcal{PT}$-symmetric potential (12) as a function of V_0 at $W_0 = 2$. The phase transition threshold is approximately $V_0 = -1.75$, which well coincides with the theoretic result $|W_0| = 0.25 - V_0$.

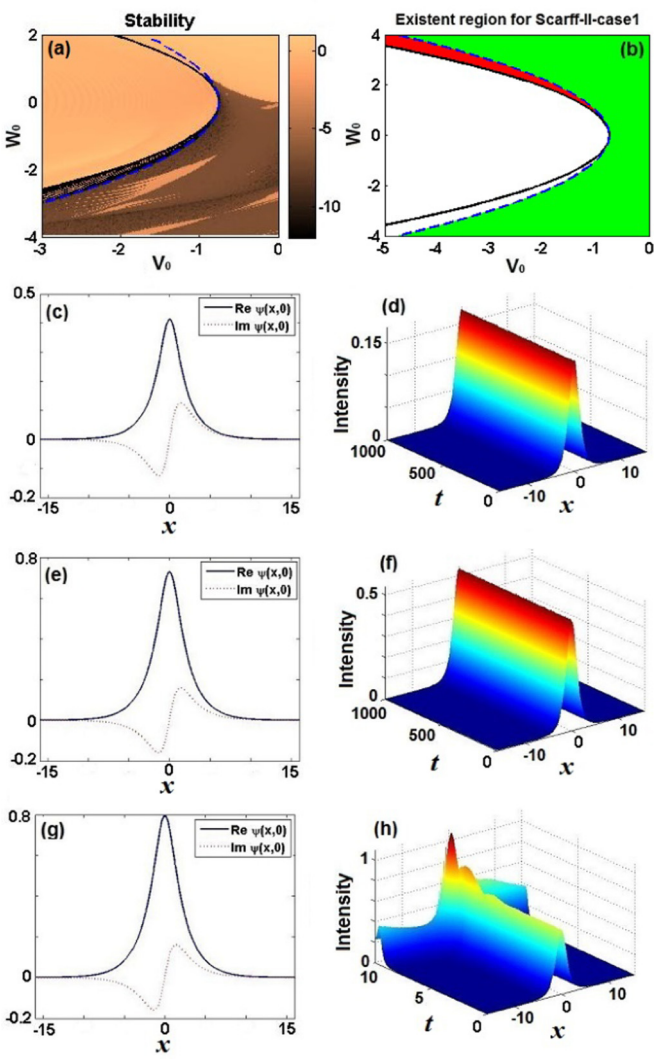

FIG. 2. (a) Stable (darker areas with smaller color values) and unstable (brighter areas with larger color values) regions of nonlinear modes (14) [determined by the maximal absolute value of imaginary parts of the linearized eigenvalue δ in Eq. (11) in the (V_0, W_0) space (common logarithmic scale), similarly hereinafter]. (b) The existence region (the shaded red and green areas) for Scarf-II-Case-1. Profile and evolution of nonlinear modes for (c), (d) $V_0 = -1, W_0 = -1.1$ (unbroken linear $\mathcal{PT}$ symmetry), (e), (f) $V_0 = -1, W_0 = -1.4$ (broken linear $\mathcal{PT}$ symmetry), (g), (h) $V_0 = -1, W_0 = -1.5$ (broken linear $\mathcal{PT}$ symmetry).

contains both entire region of broken $\mathcal{PT}$-symmetric phase and partial region of unbroken $\mathcal{PT}$-symmetric phase [see Fig. 2(b)], whereas the existence region of bright solitons (14) for Scarf-II-Case-2 is only located between the two parabolas in the upper half plane, utterly located in the region of unbroken linear $\mathcal{PT}$-symmetric phase [see Fig. 3(b)]. Moreover, we find that the strength V_0 and W_0 of the potential (12) can modulate not only amplitudes of bright solitons (14) but also the corresponding power

$$P = \int_{-\infty}^{+\infty} |\psi(x,t)|^2 dx = \frac{2}{3}\pi\phi_0,$$

which is conserved in time.

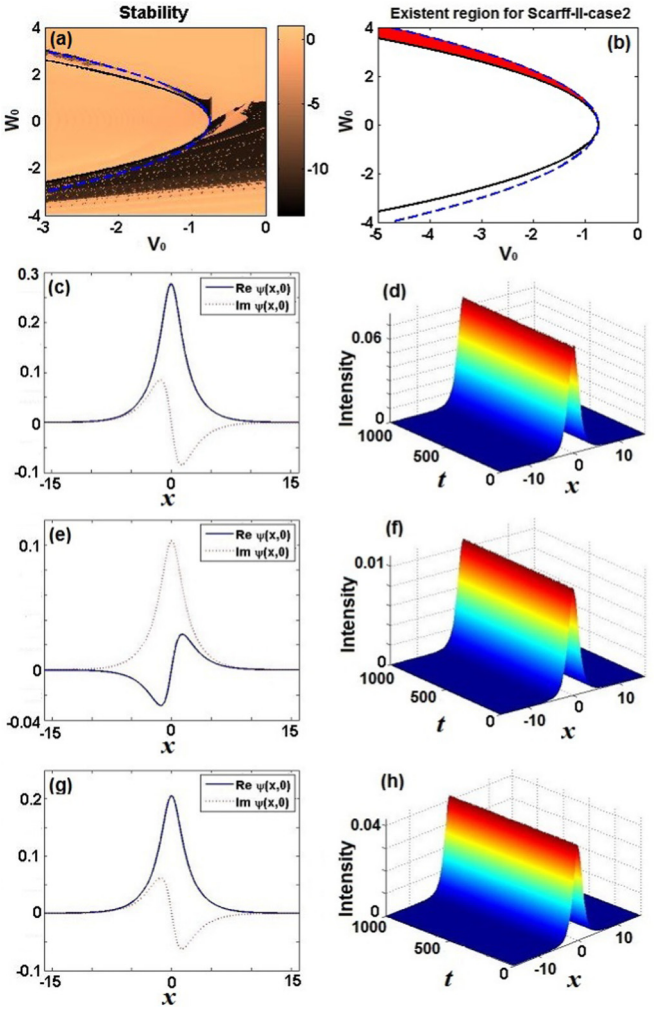

FIG. 3. (a) Stable and unstable regions of nonlinear modes (14). (b) The existence region (the shaded red area) for Scarf-II-Case-2. Profile and evolution of nonlinear modes with unbroken linear $\mathcal{PT}$ symmetry for (c), (d) $V_0 = -0.9, W_0 = 0.74$; (e), (f) $V_0 = -0.9, W_0 = 0.78$; (g), (h) $V_0 = -0.91, W_0 = 0.78$.

Stability. In the following we investigate numerically the linear stability of bright solitons (14) for the Scarf-II-Case-1 and Scarf-II-Case-2 through the direct wave propagation of initially stationary modes (14) with some 2% noise perturbation. In practice, we numerically simulate the beam propagation with the initial input $\psi(x, t = 0) = \phi(x)(1 + \epsilon)$, where $\phi(x)$ is a nonlinear mode [e.g., Eq. (14)] of Eq. (4), and ϵ is a complex broadband random perturbation. In the MATLAB program, the 2% white noise ϵ can be realized by utilizing a random matrix such as $\epsilon = 0.02\sqrt{2}[\text{rand}(N,1) - 0.5](1 + i)$, where $\text{rand}(N,1)$ returns a N-by-1 array of pseudorandom uniform values on the open interval $(0,1)$ (similarly hereinafter). Figure 2(a) for Scarf-II-Case-1 and Fig. 3(a) for Scarf-II-Case-2 exhibit the stable (darker) and unstable (brighter) regions of nonlinear localized modes (14), respectively, which are determined by the maximum absolute value of imaginary parts of the linearized eigenvalue δ in Eq. (11) in (V_0, W_0) space.

For Scarf-II-Case-1 with $V_0 = -1, W_0 = -1.1$, belonging to the region of unbroken linear $\mathcal{PT}$-symmetric phase [see

Fig. 1(a)], the corresponding nonlinear localized mode is stable [see Fig. 2(d)]. If we fix $V_0 = -1$ and change $W_0 = -1.4$ (it in fact holds for $W_0 \in (-1.25, -1.4]$), in spite of belonging to the region of broken linear $\mathcal{PT}$-symmetric phase, the corresponding nonlinear localized mode can still keep stable [see Fig. 2(g)], that is, the derivative nonlinearity can excite the broken linear $\mathcal{PT}$-symmetric phase to the unbroken nonlinear $\mathcal{PT}$-symmetric phase. If we further increase W_0 a little bit to $W_0 = -1.5$ (broken $\mathcal{PT}$-symmetric phase), the corresponding nonlinear mode begins to grow to become unstable [see Fig. 2(h)].

For the Scarf-II-Case-2, the bright solitons (14) only exist in the extremely narrow region between those two parabolas contained in the domain of unbroken $\mathcal{PT}$-symmetric phase [Fig. 3(b)]. We find the stable nonlinear mode for $V_0 = -0.9$, $W_0 = -0.74$ [Fig. 3(d)]. When we fix $V_0 = -0.9$ and increase W_0 to $W_0 = 0.78$, in which the Eq. (14) becomes

$$\phi_{\rm in}(x) = ia\sqrt{{\rm sech}x}\exp[-ib\tan^{-1}(\sinh x)] \qquad (17)$$

with $a = 0.103\,247\,113\,6, b = 0.382\,005\,025\,2$. It is easy to verify that the stationary function $\phi_{\rm in}(x)$ does not solve Eq. (4) analytically any more and its real (imaginary) part is an odd (even) function differing from the former cases, but we surprisedly find it can be stable through the direct evolution using $\phi_{\rm in}(x)$ as an initial condition with some 2% noise perturbation [see Fig. 3(f)]. When we fix $W_0 = 0.78$ and decrease V_0 a little bit to $V_0 = -0.91$, in which the solution satisfies Eq. (3) and the linear $\mathcal{PT}$-symmetric phase is unbroken, a stable nonlinear localized mode is found again [see Fig. 3(h)].

Interactions of solitons. We now investigate the interaction between two solitary waves in the $\mathcal{PT}$-symmetric Scarf-II potential. For the Scarf-II-Case-1 and $V_0 = -1$, $W_0 = -1.1$, we consider the initial condition

$$\psi(x,0) = \phi(x) + \sqrt{\frac{2}{3}\phi_0{\rm sech}(x+20)}e^{4ix}$$

with $\phi(x)$ determined by Eq. (14), as a result, the semielastic interaction is generated in which the particular nonlinear mode does not change its shape whereas the exotic incident wave becomes damped before and after interaction [see Fig. 4(a)]. When W_0 decreases a little bit to $W_0 = -1.4$, we consider the initial condition

$$\psi(x,0) = \phi(x) + \sqrt{\frac{2}{3}\phi_0{\rm sech}(x+40)}e^{10ix}$$

with $\phi(x)$ determined by Eq. (14), then a novel phenomenon occurs in collision that there exists a reflected wave when exotic incident wave interacts with the particular soliton (14) [see Fig. 4(d)]. Through repeated numerical tests, we find the reflected wave is probably related to the simultaneously increasing amplitude of the particular soliton and exotic incident wave. As W_0 decreases from -1.1 to -1.4, it is easy to verify that the amplitude (determined by ϕ_0) of the particular soliton or exotic incident wave increases and in the meantime the reflected wave begins to occur and then becomes larger and larger [see Figs. 4(a)–4(d)]. However, the nonlinear mode still does not change its shape before and after interaction. Similarly, for the Scarf-II-Case-2, we successively consider

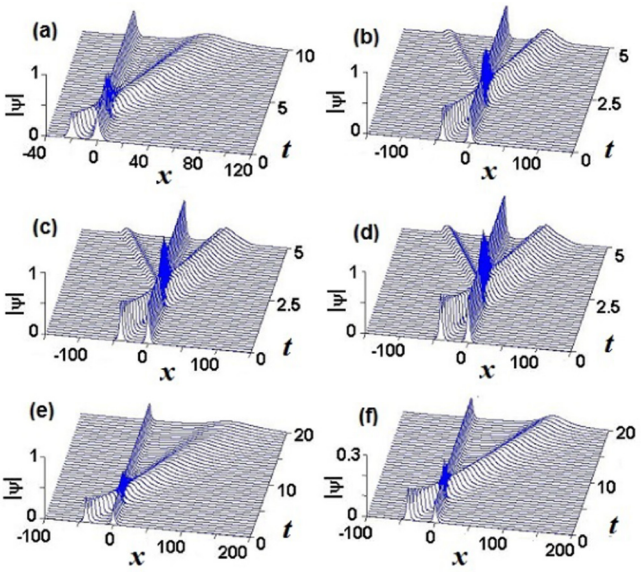

FIG. 4. Interactions of two solitary waves in Eq. (3) with the Scarf-II potential (12). (a) The solution (14) for Scarf-II-Case-1 with the wave $\sqrt{\frac{2}{3}\phi_0{\rm sech}(x+20)}e^{4ix}$ and $V_0 = -1, W_0 = -1.1$. For $V_0 = -1$, the solution (14) for Scarf-II-Case-1 with the wave $\sqrt{\frac{2}{3}\phi_0{\rm sech}(x+40)}e^{10ix}$ and (b) $W_0 = -1.2$, (c) $W_0 = -1.3$, (d) $W_0 = -1.4$. (e) The solution (14) for Scarf-II-Case-2 with the wave $\sqrt{\frac{3}{2}\phi_0{\rm sech}(x+40)}e^{4ix}$ and $V_0 = -0.9, W_0 = 0.74$. (f) The solution (14) for Scarf-II-Case-2 with the wave $\sqrt{\frac{3}{2}\phi_0{\rm sech}(x+40)}e^{4ix}$ and $V_0 = -0.9, W_0 = 0.78$.

the initial condition

$$\psi(x,0) = \phi(x) + \sqrt{\frac{3}{2}\phi_0{\rm sech}(x+40)}e^{4ix}$$

for $V_0 = -0.9, W_0 = 0.74$ and $V_0 = -0.9, W_0 = 0.78$ with $\phi(x)$ determined by Eq. (14), the similar semielastic interactions to Fig. 4(a) are generated [see Figs. 4(e), 4(f)].

To better understand the properties of nonlinear localized modes (14), we study their corresponding transverse power flow (Poynting vector)

$$S(x) = \frac{i}{2}(\psi\psi_x^* - \psi^*\psi_x) = -\frac{1}{3}\phi_0(W_0 + \phi_0){\rm sech}^2 x$$

with $\phi_0 > 0$. Signs and directions of the transverse power flow $S(x)$ are discussed in Fig. 5.

C. Excitations of nonlinear modes

Finally, we discuss the excitation of nonlinear localized modes by means of changing the potential amplitudes as the functions of time, $V_0 \to V_0(t)$ or $W_0 \to W_0(t)$ (cf. Ref. [21]). It means that we focus on the simultaneous adiabatic switching on the Scarf-II potential, governed by

$$i\psi_t + \psi_{xx} - [V(x,t) + iW(x,t)]\psi + ig(|\psi|^2\psi)_x = 0, \qquad (18)$$

where $V(x,t), W(x,t)$ are given by Eq. (12) with $V_0 \to V_0(t)$ and $W_0 \to W_0(t)$, and $V_0(t), W_0(t)$ are both chosen as the

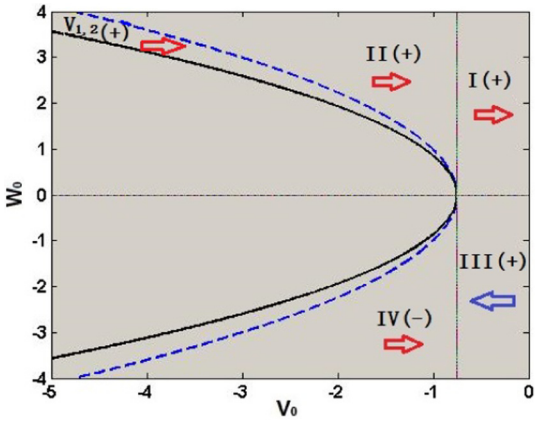

FIG. 5. Signs and directions of the transverse power flow $S(x)$ with regard to nonlinear modes (14). The dashed parabola $W_0^2 + 4V_0 + 3 = 0$, solid parabola $4W_0^2 + 12V_0 + 9 = 0$, horizontal line $W_0 = 0$ and vertical line $V_0 = -3/4$ divide the existent region of particular soliton solutions (14) into six small domains (I, II, III, IV, $V_{1,2}$ for Scarf-II-Case-1, and only $V_{1,2}$ for Scarf-II-Case-2, where + (−) denotes the positive (negative) sign of $S(x)$, and the rightward (leftward) arrow denotes the direction of power flow is from loss (gain) to gain (loss).

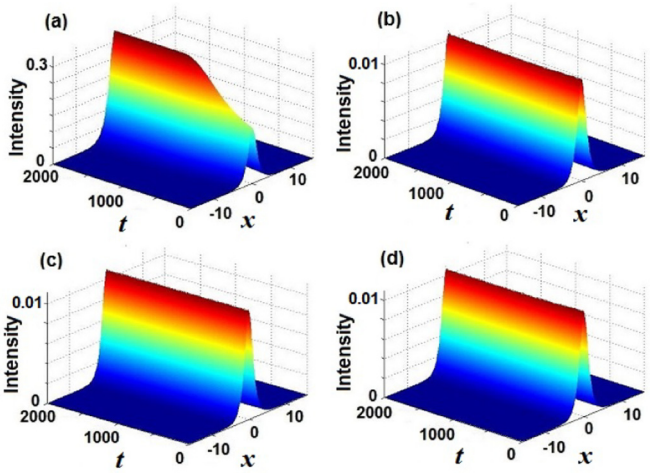

FIG. 6. Excitation of stable nonlinear localized states [cf. Eq. (18)]. (a) $V_0 = -1, W_{01} = -1.1, W_{02} = -1.4$, from stable nonlinear state belonging to unbroken linear $\mathcal{PT}$ symmetry to stable nonlinear state belonging to broken linear $\mathcal{PT}$ symmetry for Scarf-II-Case-1; (b) $V_0 = -0.9, W_{01} = 0.78, W_{02} = 0.74$, (c) $V_{01} = -0.9, V_{02} = -0.91, W_0 = 0.78$, (d) $V_{01} = -0.9, V_{02} = -0.91, W_{01} = 0.78, W_{02} = 0.74$, from stable nonlinear state to stable nonlinear state with unbroken linear $\mathcal{PT}$ symmetry for Scarf-II-Case-2.

following form

$$\epsilon(t) = \begin{cases} (\epsilon_2 - \epsilon_1)\sin(\pi t/2000) + \epsilon_1, & 0 \leqslant t < 10^3 \\ \epsilon_2, & t \geqslant 10^3 \end{cases}, \quad (19)$$

where $\epsilon_{1,2}$ are real constants. It is easy to verify that nonlinear localized modes (14) with $V_0 \to V_0(t)$ or $W_0 \to W_0(t)$ do not satisfy Eq. (18) any more, whereas the modes (14) do satisfy Eq. (18) for both the initial state $t = 0$ and excited states $t \geqslant 10^3$.

For the Scarf-II-Case-1, Fig. 6(a) exhibits the wave propagation of the nonlinear modes $\psi(x,t)$ of Eq. (18) via the initial condition given by Eq. (14) with $W_0 \to W_0(t)$ given by Eq. (19), which excites an initially stable nonlinear localized mode given by Eq. (14) for $(V_0, W_{01}) = (-1, -1.1)$ with the unbroken linear $\mathcal{PT}$-symmetric phase to another stable nonlinear localized mode given by Eq. (14) for $(V_0, W_{02}) = (-1, -1.4)$ belonging to broken linear $\mathcal{PT}$-symmetric phase. It also indicates fully that bright solitons (14) have extremely strong capacity of resisting disturbance.

For the Scarf-II-Case-2, we successively perform three types of excitations by changing potential amplitudes $V_0 \to V_0(t)$ or $W_0 \to W_0(t)$ singly or simultaneously. Similarly, Fig. 6(b) displays the wave propagation of nonlinear modes $\psi(x,t)$ of Eq. (18) using the initial condition given by Eq. (14) with $W_0 \to W_0(t)$ given by Eq. (19), which excites a stable nonlinear localized mode given by Eq. (14) for $(V_0, W_{01}) = (-0.9, 0.78)$ to another stable nonlinear localized mode given by Eq. (14) for $(V_0, W_{02}) = (-0.9, 0.74)$, both of which belong to unbroken linear $\mathcal{PT}$-symmetric phases. The property is fairly significant to find numerically or experimentally the stable nonlinear mode from a nonlinear mode due to the stability of excitation. Of course, we can also achieve the same purpose only by turning V_0 appropriately. Figure 6(c) displays the wave propagation of nonlinear mode $\psi(x,t)$ of Eq. (18) via the initial condition given by Eq. (14) with $V_0 \to V_0(t)$ given by Eq. (19), which excites a stable nonlinear localized mode given by Eq. (14) for $(V_{01}, W_0) = (-0.9, 0.78)$ to another stable nonlinear localized mode given by Eq. (14) for $(V_{02}, W_0) = (-0.91, 0.78)$, both of which belong to unbroken linear $\mathcal{PT}$-symmetric phases. Figure 6(d) shows the wave propagation of nonlinear mode $\psi(x,t)$ of Eq. (18) via the initial condition given by Eq. (14) with $V_0 \to V_0(t), W_0 \to W_0(t)$ given by Eq. (19), which excites a stable nonlinear localized mode given by Eq. (14) for $(V_{01}, W_{01}) = (-0.9, 0.78)$ to another stable nonlinear localized mode given by Eq. (14) for $(V_{02}, W_{02}) = (-0.91, 0.74)$, both of which also belong to unbroken linear $\mathcal{PT}$-symmetric phases.

IV. NONLINEAR MODES IN THE $\mathcal{PT}$-SYMMETRIC HARMONIC-HERMITE-GAUSSIAN POTENTIAL

Next we consider another physically significant potential, that is, the harmonic potential and gain-and-loss distribution of Hermite-Gaussian type

$$V(x) = \omega^2 x^2, \quad (20)$$

$$W_n(x) = \sigma H_n(\sqrt{\omega}x)[\omega x H_n(\sqrt{\omega}x) - 2n\sqrt{\omega}H_{n-1}(\sqrt{\omega}x)]e^{-\omega x^2}, \quad (21)$$

where the frequency $\omega > 0$ and real constant $\sigma > 0$ can adjust amplitudes of the harmonic potential $V(x)$ and gain-and-loss distribution $W_n(x)$, and $H_n(x) = (-1)^n e^{x^2}(d^n e^{-x^2})/(dx^n)$ represents the Hermite polynomial with n being a non-negative integer and $H_n(x) \equiv 0$ as $n < 0$. It is easy to verify that these complex potentials $V(x) + iW_n(x)$ are all $\mathcal{PT}$ symmetric for any non-negative integer n, which differ from other ones [21]. Without loss of generality, in what follows we mainly focus on the $\mathcal{PT}$-symmetric potentials (20) and (21) for $n = 0, 1, 2$.

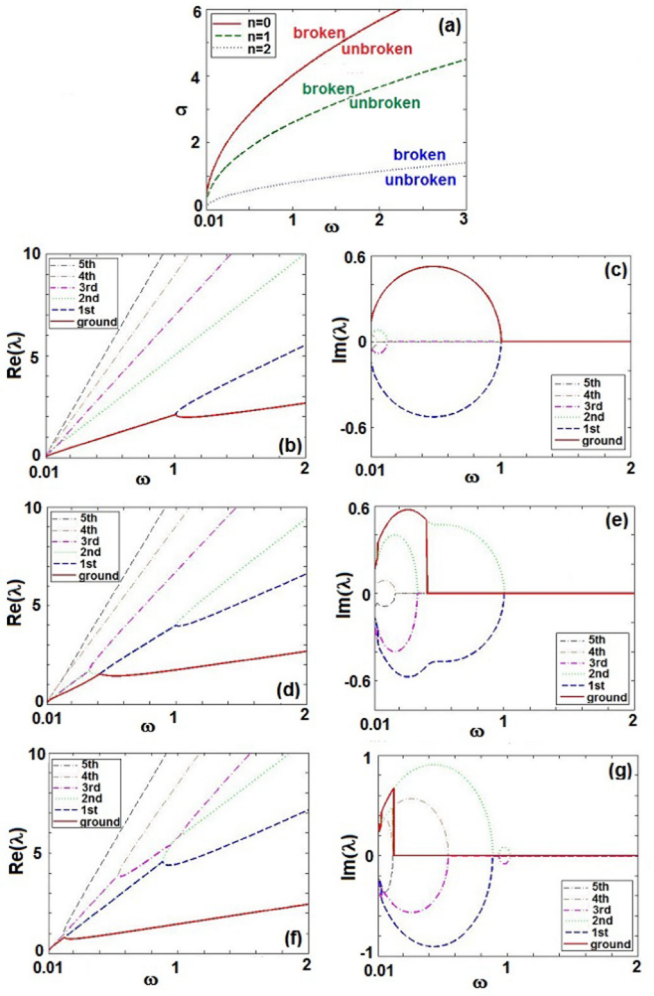

FIG. 7. (a) The unbroken (broken) $\mathcal{PT}$-symmetric phases are in the domain below (above) the phase-breaking curves [$n = 0$ (solid), $n = 1$ (dashed), $n = 2$ (dotted)] for the linear operator L in Eq. (13) with $\mathcal{PT}$-symmetric harmonic potentials (20) and gain-and-loss distributions (21). (b), (d), (f) Real and (c), (e), (g) imaginary parts of the eigenvalues λ of the linear problem (13) with $\mathcal{PT}$-symmetric potential (20) and (21) as a function of ω, at ($\sigma = 4$, $n = 0$), ($\sigma = 2.59$, $n = 1$), and ($\sigma = 0.81$, $n = 2$), respectively. The three phase transition thresholds are all approximately $\omega = 1$, in accord with the phase-breaking curves in (a).

A. Linear spectral problem

Here we investigate the linear operator L in Eq. (13) with $\mathcal{PT}$-symmetric potentials composed of $V(x)$ (20) and $W_{0,1,2}(x)$ (21), which are explicitly given by ($n = 0,1,2$)

$$W_0(x) = \sigma\omega x e^{-\omega x^2}, \tag{22a}$$

$$W_1(x) = 4\sigma\omega x(\omega x^2 - 1)e^{-\omega x^2}, \tag{22b}$$

$$W_2(x) = 4\sigma\omega x(4\omega^2 x^4 - 12\omega x^2 + 5)e^{-\omega x^2}, \tag{22c}$$

For $n = 0,1,2$, the regions of unbroken and broken linear $\mathcal{PT}$-symmetric phases on (ω,σ) space are all numerically exhibited in Fig. 7. It can be obviously observed that the ranges of unbroken linear $\mathcal{PT}$-symmetric phases gradually shrink with n increasing, which is mainly because the higher amplitude of gain-and-loss distribution $W_n(x)$ can possibly lead to the broken linear $\mathcal{PT}$-symmetric phase as n increases. For some fixed σ, we also illustrate numerically the collisions of the first six lowest discrete energy levels as the frequency ω decreases [see Figs. 7(b)–7(g)]. Notice that only the first two lowest energy levels interact with each other for $n = 0$ whereas the situations become more and more intricate with n growing.

B. Nonlinear modes and stability

For the above-mentioned $\mathcal{PT}$-symmetric potential $V(x) + iW_n(x)$ with Eqs. (20) and (21), we find a family of particular multihump soliton solutions of Eq. (4)

$$\phi_n(x) = \sqrt{\sigma}H_n(\sqrt{\omega}x)e^{-\omega x^2/2}e^{i\varphi_n(x)}, \quad \sigma > 0, \tag{23}$$

where the chemical potential in Eq. (4) is given by

$$\mu = -\omega(2n + 1),$$

and the phase function is

$$\varphi_n(x) = -\sigma\int_0^x H_n^2(\sqrt{\omega}s)e^{-\omega s^2}ds.$$

For the cases $n = 0,1,2$, we first give the regions of linear stability [cf. Eq. (11)] of nonlinear localized modes (23) in the (ω,σ) space [see Figs. 8(a1)–8(c1)]. It is more than evident that the stable regions of linear stability have the similar narrowing behaviors to the corresponding unbroken $\mathcal{PT}$-symmetric phase above on account of the rising strength of the gain-and-loss distribution $W_n(x)$ as n increases. Moreover, the stable regions of linear stability are entirely included in the regions of the corresponding unbroken $\mathcal{PT}$-symmetric phases, which indicates the derivative nonlinear term makes a negative influence on the corresponding linear $\mathcal{PT}$-symmetric phase.

We now study numerically the dynamical stability of bright solitons (23) for cases $n = 0,1,2$ through the direct wave propagation of initially stationary mode (23) for several specific amplitude parameters (ω,σ) with some 2% noise perturbation. For $n = 0$ and the fixed $\omega = 1$, we modulate σ from a very small positive number (e.g., $\sigma = 0.001$) to $\sigma = 1.1$ to perform the direct wave evolution of one-hump nonlinear modes (23) such that we obtain the stable one-hump solitons [see Figs. 8(a2), 8(a3)]. Whereas we further increase σ to $\sigma = 1.2$, the one-hump nonlinear mode (23) begins to become extremely unstable [see Fig. 8(a4)]. The main reason is that the gain-and-loss distribution $W_n(x)$ has a stronger effect on the stability of modes as σ increases. For the fixed $\sigma = 0.1$, we only change ω from 1 to 2 continuously such that we also find a series of stable one-hump solitons, although there exist some small periodic variation as ω approaches to 2 [see Fig. 8(a5)].

For $n = 1$, we can also find a family of stable two-hump solitons (23) for a fixed $\omega = 2$ and $\sigma = 0.1 \to 0.8$ [see Figs. 8(b2), 8(b3)]. Whereas we further increase σ from 0.8 to 1, the two-hump nonlinear mode (23) begins to become extremely unstable [see Fig. 8(b4)]. For a fixed $\sigma = 0.1$, we change ω from 2 to 3 continuously such that we can also find a series of stable two-hump solitons [Fig. 8(b5)]. For $n = 2$, we also have the similar results for three-hump solitons [see Figs. 8(c2)–8(c5)].

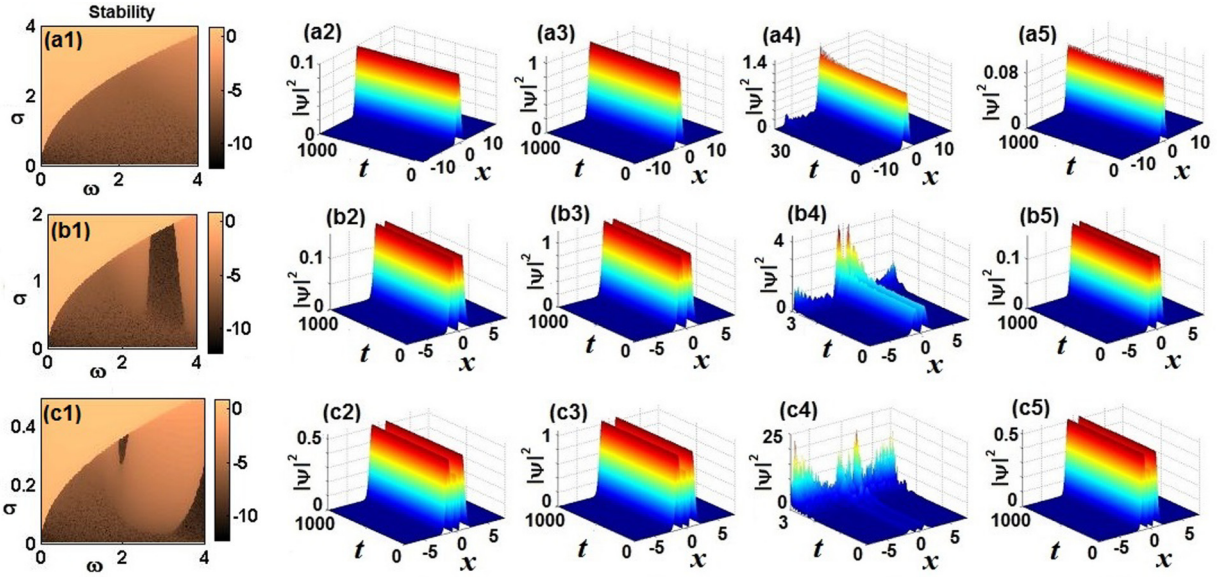

FIG. 8. Linear stability of nonlinear modes (23) for (a1) $n = 0$, (b1) $n = 1$, and (c1) $n = 2$. Evolutions of nonlinear modes (23) for one-hump ($n = 0$) with unbroken linear $\mathcal{PT}$ symmetry [(a2) $\omega = 1, \sigma = 0.1$ (stable), (a3) $\omega = 1, \sigma = 1.1$ (stable), (a4) $\omega = 1, \sigma = 1.2$ (unstable), (a5) $\omega = 2, \sigma = 0.1$ (periodically varying)], two-hump ($n = 1$) with unbroken linear $\mathcal{PT}$ symmetry [(b2) $\omega = 2, \sigma = 0.1$ (stable), (b3) $\omega = 2, \sigma = 0.8$ (stable), (b4) $\omega = 2, \sigma = 1$ (unstable), (b5) $\omega = 3, \sigma = 0.1$ (stable)], three-hump ($n = 2$) with unbroken linear $\mathcal{PT}$ symmetry [(c2) $\omega = 2, \sigma = 0.1$ (stable), (c3) $\omega = 2, \sigma = 0.2$ (stable), (c4) $\omega = 2, \sigma = 0.3$ (unstable), (c5) $\omega = 3, \sigma = 0.1$ (stable)].

Next we investigate the interactions of bright solitons (23) in the $\mathcal{PT}$-symmetric potential $V(x) + iW_n(x)$ with (20) and (21). For $n = 0$ and $\omega = 1, \sigma = 0.1$, we consider the initial condition

$$\psi(x,0) = \phi(x) + 0.8\sqrt{\sigma}e^{-\omega(x+10)^2/2}e^{i\varphi(x)}$$

with $\phi(x)$ determined by Eq. (23), as a result the elastic interaction is generated in which neither the particular one-hump nonlinear mode nor exotic periodic incident wave change their shapes before and after interaction [see Fig. 9(a)]. When σ becomes large to $\sigma = 1.1$, we consider the initial condition

$$\psi(x,0) = \phi(x) + 0.5\sqrt{\sigma}e^{-\omega(x+10)^2/2}e^{i\varphi(x)}$$

with $\phi(x)$ determined by Eq. (23), then a novel phenomenon occurs in collision that there exists a weak reflected wave when the exotic incident wave interacts with the particular one-hump soliton (23) [see Fig. 9(b)], which is probably related to the increasing amplitude or strength of the particular one-hump soliton (23). However, the particular one-hump

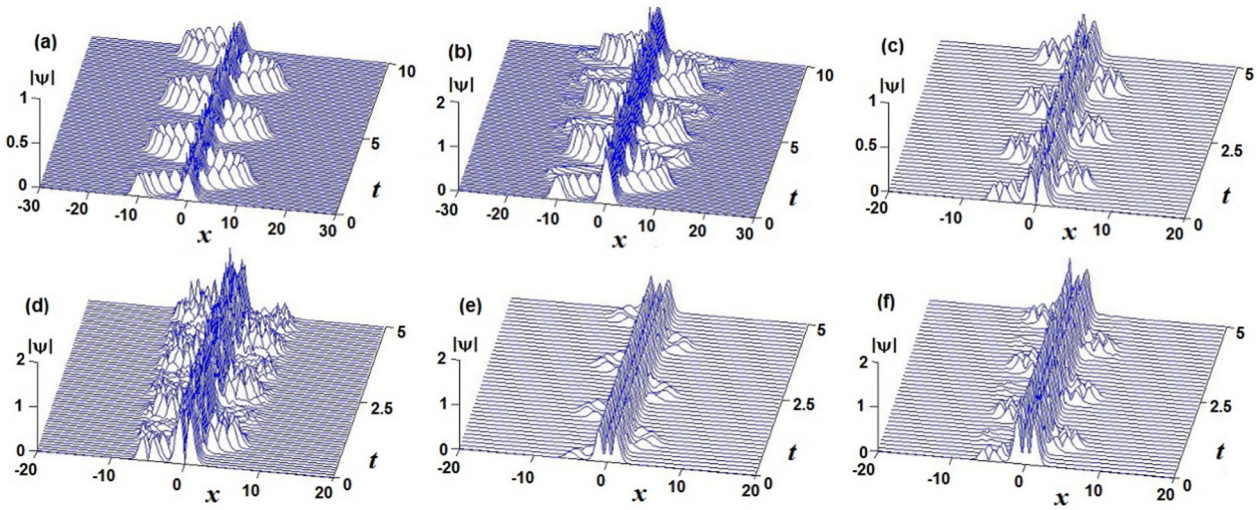

FIG. 9. Interactions of two solitary waves in Eq. (3) with the potential (20) and (21). (a) The solution (23) for $n = 0$ with the wave $0.8\sqrt{\sigma}e^{-\omega(x+10)^2/2}e^{i\varphi(x)}$ and $\omega = 1, \sigma = 0.1$. (b) The solution (23) for $n = 0$ with the wave $0.5\sqrt{\sigma}e^{-\omega(x+10)^2/2}e^{i\varphi(x)}$ and $\omega = 1, \sigma = 1.1$. (c) The solution (23) for $n = 1$ with the wave $\sqrt{\sigma\omega}(x+5)e^{-\omega(x+5)^2/2}e^{i\varphi(x)}$ and $\omega = 2, \sigma = 0.1$. (d) The solution (23) for $n = 1$ with the wave $\sqrt{\sigma\omega}(x+5)e^{-\omega(x+5)^2/2}e^{i\varphi(x)}$ and $\omega = 2, \sigma = 0.8$. (e) The solution (23) for $n = 2$ with the wave $0.5\sqrt{\sigma}e^{-\omega(x+5)^2/2}e^{i\varphi(x)}$ and $\omega = 2, \sigma = 0.1$. (f) The solution (23) for $n = 2$ with the wave $\sqrt{\sigma\omega}(x+5)e^{-\omega(x+5)^2/2}e^{i\varphi(x)}$ and $\omega = 2, \sigma = 0.2$.

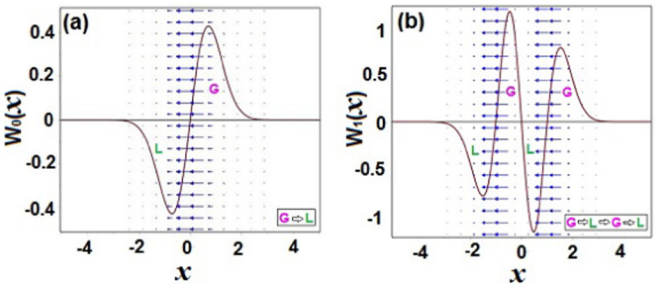

FIG. 10. (a) The direction of the transverse power flow for $n = 0$ is from the gain to loss. (b) The direction of the transverse power flow for $n = 1$ is first from the gain to loss, then from the loss to gain, finally from the gain to loss again (from left to right). Here, $W_0(x)$ only has one root $x = 0$ and $W_1(x)$ has three roots $x = 0, \pm 1$. The left arrows and its lengths denote respectively negative directions and strengths of the transverse power flow $S_{0,1}(x)$ with regard to nonlinear modes (23). G (L) denotes the gain (loss) distribution of $W_{0,1}(x)$. Other parameters are $\omega = \sigma = 1$.

nonlinear mode still doesn't change its shape before and after interaction. Similarly, for $n = 1$, we successively consider the initial condition

$$\psi(x,0) = \phi(x) + \sqrt{\sigma\omega}(x+5)e^{-\omega(x+5)^2/2}e^{i\varphi(x)}$$

for $\omega = 2, \sigma = 0.1$ and $\omega = 2, \sigma = 0.8$ with $\phi(x)$ determined by Eq. (23), the similar elastic interactions between the particular two-hump nonlinear modes and exotic periodic incident waves to Fig. 9(a) are generated [see Figs. 9(c), 9(d)]. For $n = 2$, the similar elastic interactions between the particular three-hump nonlinear modes and exotic periodic incident waves are generated [see Figs. 9(e), 9(f)].

In order to further understand the properties of the stationary nonlinear localized mode (23), we also check the corresponding transverse power flow (Poynting vector)

$$S_n(x) = -\sigma^2 H_n^4(\sqrt{\omega}x)e^{-2\omega x^2}$$

with $\omega > 0$ and $\sigma > 0$. Notice that the signs of the transverse power flow $S_n(x)$ always keep negative definite for any n. For $n = 0$, the power always flows in one direction, i.e., from the gain toward the loss domain [see Fig. 10(a)]. However, the directions of the power flow for $n = 1$ are so complicated, that is (from the negative infinite to positive infinite), first from the gain to loss, then from the loss to gain, finally from the gain to loss domain again [see Fig. 10(b), the total direction is from the gain to loss]. Similar more complicated results hold for $n = 2$ and specifically not repeat them.

C. Excitations of nonlinear modes

Finally, we investigate the excitation of stable nonlinear modes by means of changing the potential amplitudes $\omega \to \omega(t)$ or $\sigma \to \sigma(t)$, which means that we exert simultaneous adiabatic switching on the harmonic potential (20) and gain-and-loss distribution (21), modeled by Eq. (18), where $V(x,t), W(x,t)$ are given by Eq. (20) and Eq. (21) with $\omega \to \omega(t)$ and $\sigma \to \sigma(t)$. We assume that $\omega(t), \sigma(t)$ are all taken as the same form as Eq. (19) [i.e., $\epsilon(t)$ can be replaced with $\omega(t)$ or $\sigma(t)$]

$$\omega(t) = \begin{cases} (\omega_2 - \omega_1)\sin(\pi t/2000) + \omega_1, & 0 \leqslant t < 10^3 \\ \omega_2, & t \geqslant 10^3 \end{cases} \quad (24)$$

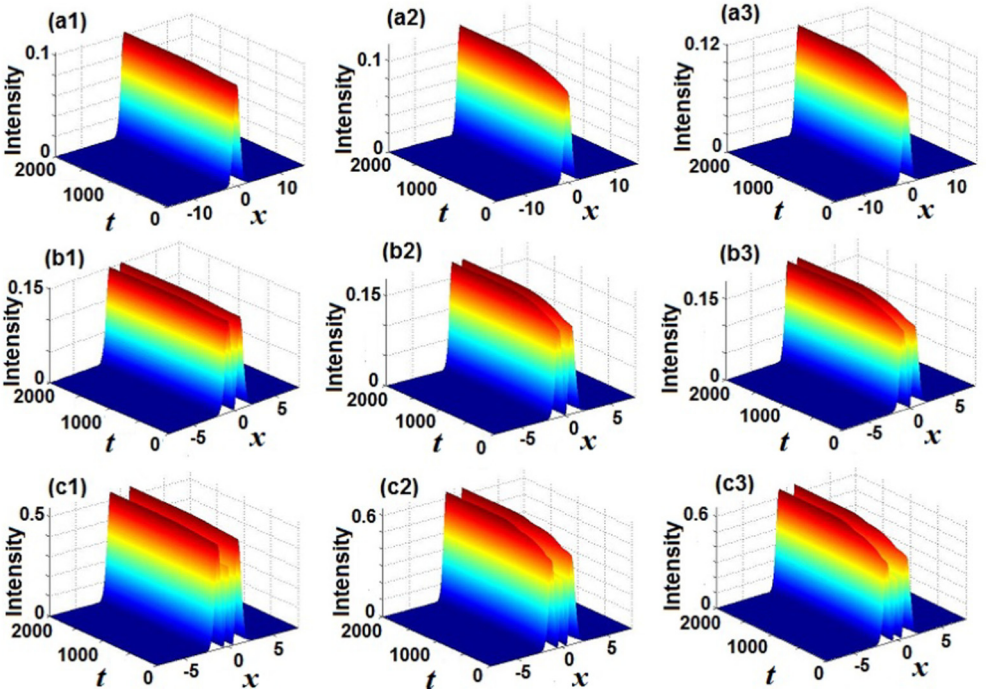

FIG. 11. Excitation of stable nonlinear localized states [cf. Eq. (18)] for $n = 0$ [(a1) $\omega = 1, \sigma_1 = 0.1, \sigma_2 = 1.1$, (a2) $\omega_1 = 1, \omega_2 = 2, \sigma = 0.1$, (a3) $\omega_1 = 1, \omega_2 = 2, \sigma_1 = 0.1, \sigma_2 = 1.1$]; $n = 1$ [(b1) $\omega = 2, \sigma_1 = 0.1, \sigma_2 = 0.8$, (b2) $\omega_1 = 2, \omega_2 = 3, \sigma = 0.1$, (b3) $\omega_1 = 2, \omega_2 = 3, \sigma_1 = 0.1, \sigma_2 = 0.8$]; $n = 2$ [(c1) $\omega = 2, \sigma_1 = 0.1, \sigma_2 = 0.2$, (c2) $\omega_1 = 2, \omega_2 = 3, \sigma = 0.1$, (c3) $\omega_1 = 2, \omega_2 = 3, \sigma_1 = 0.1, \sigma_2 = 0.2$].

and

$$\sigma(t) = \begin{cases} (\sigma_2 - \sigma_1)\sin(\pi t/2000) + \sigma_1, & 0 \leqslant t < 10^3 \\ \sigma_2, & t \geqslant 10^3 \end{cases}, \quad (25)$$

where ω_1 (or σ_1) and ω_2 (or σ_2) denote some initial (or final) values of the excitation function $\omega(t)$ [or $\sigma(t)$], respectively.

We have the similar results that the nonlinear localized modes (23) with $\omega \to \omega(t)$ or $\sigma \to \sigma(t)$ do not satisfy Eq. (18) any more, whereas the nonlinear modes (23) indeed satisfy Eq. (18) for the initial state $t = 0$ and excited states $t \geqslant 10^3$.

For $n = 0,1,2$, we numerically perform three distinct types of excitations by changing the potential amplitudes $\omega \to \omega(t), \sigma \to \sigma(t)$, or both, respectively. For $n = 0$, Fig. 11(a1) exhibits the wave evolution of nonlinear modes $\psi(x,t)$ of Eq. (18) via the initial condition given by Eq. (23) with $\sigma \to \sigma(t)$ given by Eq. (25), which excites a stable one-hump nonlinear localized mode given by Eq. (23) for $(\omega,\sigma_1) = (1,0.1)$ to another stable one-hump nonlinear localized mode given by Eq. (23) for $(\omega,\sigma_2) = (1,1.1)$, which both belong to unbroken linear $\mathcal{PT}$-symmetric phase [all mentioned points (ω,σ) enjoy the same property of unbroken linear $\mathcal{PT}$-symmetric phase hereafter]. Figure 11(a2) displays the wave propagation of the nonlinear modes $\psi(x,t)$ of Eq. (18) via the initial condition given by Eq. (23) with $\omega \to \omega(t)$ singly given by Eq. (24), which excites a initially stable one-hump nonlinear localized mode given by Eq. (23) for $(\omega_1,\sigma) = (1,0.1)$ to another stable one-hump nonlinear localized mode given by Eq. (23) for $(\omega_2,\sigma) = (2,0.1)$. Figure 11(a3) displays the wave propagation of the nonlinear modes $\psi(x,t)$ of Eq. (18) via the initial condition given by Eq. (23) with $\omega \to \omega(t)$ and $\sigma \to \sigma(t)$ simultaneously given by Eqs. (24) and (25), which excites a stable one-hump nonlinear localized mode given by Eq. (23) for $(\omega_1,\sigma_1) = (1,0.1)$ to another stable one-hump nonlinear localized mode given by Eq. (23) for $(\omega_2,\sigma_2) = (2,1.1)$.

Similarly for $n = 1$, we excite a stable two-hump nonlinear localized mode given by Eq. (23) for $(\omega,\sigma) = (2,0.1)$ to another stable two-hump nonlinear localized mode given by Eq. (23) for $(\omega,\sigma) = (2,0.8),(\omega,\sigma) = (3,0.1)$, and $(\omega,\sigma) = (3,0.8)$, respectively [see Figs. 11(b1)–11(b3)].

For $n = 2$, we also excite a stable three-hump nonlinear localized mode given by Eq. (23) for $(\omega,\sigma) = (2,0.1)$ to another stable three-hump nonlinear localized mode given by Eq. (23) for $(\omega,\sigma) = (2,0.2),(\omega,\sigma) = (3,0.1)$, and $(\omega,\sigma) = (3,0.2)$, respectively [see Figs. 11(c1)–11(c3)]. These stable excitations also shows that bright solitons (23) have extremely strong capacity of resisting disturbance.

V. CONCLUSIONS AND DISCUSSIONS

In conclusion, some stable bright solitons have been found in the derivative nonlinear Schrödinger equation with $\mathcal{PT}$-symmetric Scarf-II and harmonic-Hermite-Gaussian potentials. First, the linear $\mathcal{PT}$-symmetric breaking curves are numerically exhibited. Second, in the presence of derivative nonlinearity, such $\mathcal{PT}$-symmetric solitons are shown to be stable through the linear stability analysis and direct wave propagation with some noise perturbation. Moreover, the semielastic interactions between particular bright solitons and exotic incident waves are illustrated and the transverse power flows are also checked in detail. Finally, the soliton excitations are also studied including from a stable nonlinear mode with unbroken linear $\mathcal{PT}$-symmetric phase to another stable nonlinear mode with broken linear $\mathcal{PT}$-symmetric phase and from a stable nonlinear mode to another stable nonlinear mode. In fact, we may change the nonlinear coefficient g as the function of space such that the stable solitons can also be generated. The idea used in this paper can also be extended to the coupled DNLS equations with $\mathcal{PT}$-symmetric potentials.

ACKNOWLEDGMENTS

The authors would like to thank the referees for the valuable suggestions. This work was supported by the NSFC under Grant No. 11571346 and and the Youth Innovation Promotion Association CAS.

[1] G. P. Agrawal, *Nonlinear Fibre Optics*, 5th ed. (Academic Press, New York, 2014).
[2] N. Tzoar and M. Jain, Phys. Rev. A **23**, 1266 (1981).
[3] D. Anderson and M. Lisak, Phys. Rev. A **27**, 1393 (1983).
[4] X.-J. Chen and W. K. Lam, Phys. Rev. E **69**, 066604 (2004).
[5] K. Mio, T. Ogino, K. Minami, and S. Takeda, J. Phys. Soc. Jpn. **41**, 265 (1976); E. Mjolhus, J. Plasma Phys. **16**, 321 (1976).
[6] M. S. Ruderman, J. Plasma Phys. **67**, 271 (2002).
[7] K. H. Spatchek, P. K. Shukla, and M. Y. Yu, Nucl. Fusion **18**, 290 (1977); H. Steudel, J. Phys. A **36**, 1931 (2003).
[8] D. J. Kaup and A. C. Newell, J. Math. Phys. **19**, 798 (1978).
[9] H. H. Chen, Y. C. Lee, and C. S. Liu, Phys. Scr. **20**, 490 (1979).
[10] T. Kawata, N. Kobayashi, and H. Inoue, J. Phys. Soc. Jpn. **46**, 1008 (1979).
[11] L. Bergé, Phys. Plasmas **4**, 1227 (1997); L. Bergé and S. Skupin, Discrete Contin. Dyn. Syst. **23**, 1099 (2009).
[12] L. Bergé *et al.*, J. Phys. A: Math. Gen. **29**, 3581 (1996).
[13] J. S. Hesthaven *et al.*, J. Phys. A: Math. Gen. **30**, 8207 (1997).
[14] Y. S. Kivshar and G. P. Agrawal, *Optical Solitons: From Fibers to Photonic Crystals* (Academic, San Diego, 2003).
[15] J. Belmonte-Beitia, V. M. Pérez-Garcia, V. Vekslerchik, and P. J. Torres, Phys. Rev. Lett. **98**, 064102 (2007).
[16] Z. Yan, Phys. Lett. A **374**, 672 (2010); **374**, 4838 (2010).
[17] Z. Yan and D. Jiang, Phys. Rev. E **85**, 056608 (2012); Z. Yan and V. V. Konotop, *ibid.* **80**, 036607 (2009); Z. Yan, Nonlinear Dyn. **79**, 2515 (2015); Y. Yang, Z. Yan, and D. Mihalache, J. Math. Phys. **56**, 053508 (2015).
[18] S. A. Ponomarenko and G. P. Agrawal, Phys. Rev. Lett. **97**, 013901 (2006).
[19] V. N. Serkin, A. Hasegawa, and T. L. Belyaeva, Phys. Rev. Lett. **98**, 074102 (2007).
[20] Z. H. Musslimani, K. G. Makris, R. El-Ganainy, and D. N. Christodoulides, Phys. Rev. Lett. **100**, 030402 (2008).
[21] Z. Yan *et al.*, arXiv:1009.4023; Z. Yan, Phil. Trans. R. Soc. A **371**, 20120059 (2013); Z. Wen and Z. Yan, Phys. Lett. A **379**, 2025 (2015); Z. Yan, Z. Wen, and C. Hang, Phys. Rev. E **92**,

022913 (2015); Z. Yan, Y. Chen, and Z. Wen, Chaos **26**, 083109 (2016); Z. Yan, Z. Wen, and V. V. Konotop, Phys. Rev. A **92**, 023821 (2015).
[22] D. A. Zezyulin and V. V. Konotop, Phys. Rev. A **85**, 043840 (2012); Phys. Rev. Lett. **108**, 213906 (2012).
[23] C. H. Tsang, B. A. Malomed, and K. W. Chow, Phys. Rev. E **84**, 066609 (2011).
[24] F. K. Abdullaev, V. V. Konotop, M. Salerno, and A. V. Yulin, Phys. Rev. E **82**, 056606 (2010).
[25] V. E. Lobanov, O. V. Borovkova, and B. A. Malomed, Phys. Rev A **90**, 053820 (2014); J. Yang, Phys. Rev. E **91**, 023201 (2015).
[26] H. Wang and J. Wang, Opt. Express **19**, 4030 (2011).
[27] Z. Lu and Z. Zhang, Opt. Express **19**, 11457 (2011).
[28] S. Hu, X. Ma, D. Lu, Z. Yang, Y. Zheng, and W. Hu, Phys. Rev. A **84**, 043818 (2011).
[29] X. Zhu *et al.*, Opt. Lett. **36**, 2680 (2011).
[30] S. Nixon, L. Ge, and J. Yang, Phys. Rev. A **85**, 023822 (2012).
[31] C. Li, H. Liu, and L. Dong, Opt. Express **20**, 16823 (2012).
[32] A. Ruschhaupt, F. Delgado, and J. G. Muga, J. Phys. A **38**, L171 (2005).
[33] R. El-Ganainy *et al.*, Opt. Lett. **32**, 2632 (2007).
[34] C. M. Bender and S. Boettcher, Phys. Rev. Lett. **80**, 5243 (1998); C. M. Bender, Rep. Prog. Phys. **70**, 947 (2007).
[35] A. Guo, G. J. Salamo, D. Duchesne, R. Morandotti, M. Volatier-Ravat, V. Aimez, G. A. Siviloglou, and D. N. Christodoulides, Phys. Rev. Lett. **103**, 093902 (2009).
[36] C. E. Rueter *et al.*, Nature Phys. **6**, 192 (2010).
[37] A. Regensburger *et al.*, Nature (London) **488**, 167 (2012).
[38] Z. Ahmed, Phys. Lett. A **282**, 343 (2001).
[39] Y. Chen and Z. Yan, Sci. Rep. **6**, 23478 (2016).
[40] G. Castaldi, S. Savoia, V. Galdi, A. Alù, N. Engheta, Phys. Rev. Lett. **110**, 173901 (2013).
[41] A. Regensburger, M.-A. Miri, C. Bersch, J. Näger, G. Onishchukov, D. N. Christodoulides, and U. Peschel, Phys. Rev. Lett. **110**, 223902 (2013); B. Peng *et al.*, Nature Phys. **10**, 394 (2014).
[42] M. F. Saleh, A. Marini, and F. Biancalana, Phys. Rev. A **89**, 023801 (2014).
[43] A. Biswas *et al.*, *Mathematical Therory of Dispersion-Managed Optical Solitons* (Higher Education Press, Beijing, 2010).
[44] A. E. Siegman, *Lasers* (University Science Books, Sausalito, 1986).
[45] E. A. Ultanir, G. I. Stegeman, and D. N. Christodoulides, Opt. Lett. **29**, 845 (2004).
[46] C. Coste, Eur. Phys. J. B **1**, 245 (1998).